Check for updates

STRUCTURAL BIOLOGY
ISSN 2059-7983

Structural basis of ligand recognition and transport by Sfh2, a yeast phosphatidylinositol transfer protein of the Sec14 superfamily

Lin Chen, Lingchen Tan and Young Jun Im*

College of Pharmacy, Chonnam National University, Gwangju 61186, Republic of Korea. *Correspondence e-mail: imyoungjun@jnu.ac.kr

Received 15 February 2022
Accepted 25 May 2022

Edited by B. Kobe, University of Queensland, Australia

Keywords: lipid transport; yeast Sfh2; Sec14; phosphatidylinositol; squalene; lipid-transfer proteins.

PDB references: Sfh2, apo form, closed conformation, 7wwe; complex with squalene, closed conformation, 7wwd; complex with PtdIns, closed conformation, 7wvt; complex with PtdIns, open conformation, 7wwg

Supporting information: this article has supporting information at journals.iucr.org/d

Sec14-like phosphatidylinositol transfer proteins (PITPs) are involved in lipid metabolism and phosphatidylinositol 4-phosphate signaling by transporting phosphatidylinositol (PI) and a secondary ligand between the organellar membranes in eukaryotes. Yeast Sfh2 is a PITP that transfers PI and squalene without phosphatidylcholine transfer activity. To investigate the structural determinants for ligand specificity and transport in Sfh2, crystal structures of Sfh2 in complex with PI and squalene were determined at 1.5 and 2.4 Å resolution, respectively. The inositol head group of PI is recognized by highly conserved residues around the pocket entrance. The acyl chains of PI bind into a large hydrophobic cavity. Squalene is accommodated in the bottom of the cavity entirely by hydrophobic interactions. The binding of PI and squalene are mutually exclusive due to their overlapping binding sites, correlating with the role in lipid exchange. The binding mode of PI is well conserved in Sfh family proteins. However, squalene binding is unique to the Sfh2 homolog due to the specific hydrophobic residues forming a shape-complementary binding pocket. Recombinant apo Sfh2 forms a homodimer *in vitro* by the hydrophobic interaction of the gating α10–α11 helices in an open conformation. Ligand binding closes the lid and dissociates the dimer into monomers. This study reveals the structural determinants for the recognition of the conserved PI and a secondary ligand, squalene, and provides implications for the lipid-transfer function of Sfh2.

1. Introduction

Different lipids are distributed unevenly between cellular membrane compartments by vesicular transport or non-vesicular pathways medicated by lipid-transfer proteins (Wong *et al.*, 2019). Phosphatidylinositol (PI) is an essential phospholipid in eukaryotes and serves as a metabolic precursor of phosphoinositides, which are phosphorylated derivatives of PI. PI is synthesized in the endoplasmic reticulum (ER) and is subsequently transported to the Golgi complex and the plasma membrane, where it is converted to phosphoinositides by the activities of positionally specific PI kinases (Dickson & Hille, 2019; Pemberton *et al.*, 2020). The different phosphoinositide species are concentrated in the cytoplasmic leaflets of various organellar membranes and serve as organelle markers (Dickson & Hille, 2019). Phosphoinositides modulate a wide range of cellular processes, including receptor signaling, transcription, lipid metabolism and membrane trafficking (Balla, 2013).

Yeast Sec14 is a phosphatidylinositol transfer protein (PITP) that has been proposed to transport PI in the ER to the PI 4-OH kinases (PI4Ks) in the plasma membrane and in the Golgi membranes for the synthesis of phosphatidylinositol 4-phosphate [PI(4)P] (Strahl & Thorner, 2007; Schaaf *et al.*,

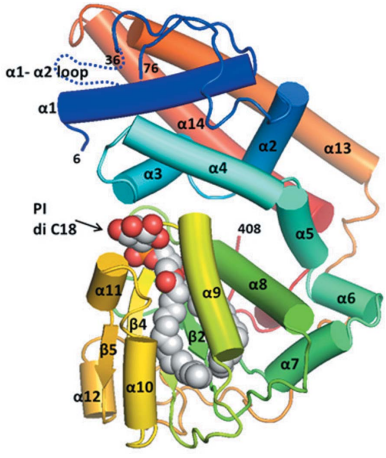

2008). Sec14 executes an essential function in yeast, integrating various aspects of lipid metabolism with PI(4)P signaling in the trans-Golgi network/endosomal system (Khan *et al.*, 2021). Budding yeast has six Sec14-like PITPs: Sec14, Sfh1, Sfh2, Sfh3, Sfh4 and Sfh5. They have heterotypic lipid-exchange activities, presenting PI to PI4K on a membrane surface, thereby boosting PI(4)P synthesis and leading to diverse biological outcomes (Grabon *et al.*, 2019). The residues that recognize the head group of PI are conserved throughout the Sec14 superfamily, whereas the residues that recognize the secondary ligands are divergent (Tripathi *et al.*, 2019). Sec14 and Sfh1 are PI/phosphatidylcholine (PC) exchangers (Schaaf *et al.*, 2008). Sfh2 and Sfh3 transport PI in exchange for squalene and ergosterol, respectively (Tripathi *et al.*, 2019; Holič *et al.*, 2014). Sfh4 binds PI, but its stimulatory activity of phosphatidylserine decarboxylation does not require PI transfer activity (Wang *et al.*, 2020). Unlike the other PITPs, Sfh5 is a heme-binding protein and does not function as a PITP even though it binds PI (Khan *et al.*, 2020).

Sfh2 (Sec14 homolog 2) is basically a cytosolic protein that also localizes to endosomes, lipid droplets and the ER (Li *et al.*, 2000; Schnabl *et al.*, 2003; Desfougères *et al.*, 2008). Sfh2 is distantly related to other Sec14 family proteins, sharing 24–27% amino-acid sequence similarity. Sfh2 influences membrane metabolism and controls vesicle transport from the trans-Golgi network (Wong *et al.*, 2005). Squalene, a direct precursor of ergosterol synthesis, is an inert hydrocarbon and is synthesized by the condensation of two farnesyl pyrophosphate molecules by squalene synthase in the ER. Sfh2 is known to transfer squalene *in vitro*, but how the transport function of PI and squalene relates to its biological outcome is not known (Tripathi *et al.*, 2019). In addition, the structural determinants for the unique recognition of squalene by the Sfh2 homolog are not clear.

In this study, in order to obtain structural insights into the lipid specificity and lipid-transfer mechanism of Sfh2, we determined structures of Sfh2 in the apo form and in complex with PI and squalene. The overall structures and the binding mode of PI are well conserved in Sfh proteins. The binding of squalene is unique to the Sfh2 homolog due to the presence of specific hydrophobic residues forming a shape-complementary binding pocket. This study reveals the structural determinants for ligand recognition and provides implications for the lipid-transfer function of Sfh2.

2. Materials and methods

2.1. Cloning of yeast Sfh2

The full-length gene for Sfh2 (UniProt ID Q06705) was amplified by polymerase chain reaction (PCR) using *S. cerevisiae* genomic DNA as a template. The PCR product for Sfh2 was subcloned into the NcoI/XhoI sites of a modified pHIS2 vector. The Sfh2 was tagged with an N-terminal hexahistidine tag followed by a thrombin protease cleavage site (LVPR/GS). Sfh2 was predicted to have a long α1–α2 loop which was susceptible to proteolytic degradation. To improve the crystallization properties and diffraction quality of Sfh2, we constructed a deletion mutant in the α1–α2 loop (Δ44–49 and Δ60–65). *Escherichia coli* strain BL21(DE3) cells transformed with the plasmid encoding the modified Sfh2 were grown to an OD_{600} of 0.8 at 37°C in LB medium. The cells were induced by the addition of isopropyl β-D-1-thiogalactopyranoside to a final concentration of 0.5 m*M* and were incubated for 12 h overnight at 20°C prior to harvesting.

2.2. Protein expression and purification

Cells expressing Sfh2 were resuspended in 2× PBS buffer containing 20 m*M* imidazole (lysis buffer) and lysed by sonication. The supernatant containing the His-tagged Sfh2 was loaded onto an Ni–NTA affinity column. The Ni–NTA column was thoroughly washed with lysis buffer. The target protein was eluted from the column using a buffer consisting of 100 m*M* Tris–HCl pH 8.0 (final), 300 m*M* imidazole. The eluate was concentrated to 10 mg ml^{-1} using Amicon Ultra-15 centrifugal filters. The His tag was cleaved using ten international units (IU) of thrombin protease (Reyon Pharmaceutical) per 10 mg of recombinant protein. The cleaved sample was subjected to size-exclusion chromatography (SEC) on a HiLoad Superdex 200 column equilibrated with 20 m*M* Tris–HCl pH 8.0, 150 m*M* NaCl. The fractions containing Sfh2 were collected and concentrated to 10 mg ml^{-1} using centrifugal filters for use in crystallization.

2.3. Crystallization and crystallographic analysis

Preliminary crystallization experiments were carried out at 22°C in 96-well crystallization plates using custom crystallization screening solutions by dispensing 0.8 µl protein solution and 0.8 µl precipitant solution. Apo Sfh2 crystals were grown in 0.1 *M* MES pH 6.0, 30% polyethylene glycol (PEG) 3350, 0.1 *M* NaCl. Crystals with dimensions of 0.1 × 0.1 × 0.1 mm appeared in two weeks. For crystallization of the Sfh2–PI complex, purified Sfh2 was mixed with a fivefold molar ratio of PI liposomes and incubated at room temperature for 2 h. The monomeric fraction of the Sfh2–PI complex was isolated by SEC. Crystals of the complex were grown in 0.1 *M* MES pH 6.0, 30% PEG 1000 in two days. For purification of the Sfh2–squalene complex, squalene (Sigma–Aldrich, catalog No. S3626) dissolved in dimethyl sulfoxide was added to the purified Sfh2 protein and incubated for 2 h prior to separation of the Sfh2–squalene complex by SEC. Crystals of the Sfh2–squalene complex appeared after two days using a solution consisting of 0.1 *M* HEPES pH 7.0, 0.1 *M* KNO_3, 30% PEG 3350.

The crystals of Sfh2 were cryoprotected in reservoir solution supplemented with 10% glycerol and flash-cooled by immersion in liquid nitrogen. Crystals were preserved in a cryogenic nitrogen gas stream (~100 K) during diffraction experiments. Native diffraction data for the Sfh2 crystals were collected at a fixed wavelength of 0.97950 Å using an ADSC Q270 CCD detector on beamline 7A at Pohang Light Source (PLS), Pohang Accelerator Laboratory. All data were processed and scaled using *HKL*-2000. The structures of

Table 1
Data-collection and refinement statistics.

Values in parentheses are for the outer shell.

	Sfh2–PI (closed form)	Sfh2–PI (open form)	Sfh2–squalene (closed form)	Apo Sfh2 (closed form)
Data collection				
Diffraction source	7A, PLS	7A, PLS	7A, PLS	7A, PLS
Wavelength (Å)	0.97950	0.97950	0.97950	0.97950
Space group	$P2_12_12$	$P4_32_12$	$P2_1$	$P2_1$
a, b, c (Å)	74.5, 117.1, 42.6	75.1, 75.1, 146.8	43.4, 78.3, 54.2	42.9, 78.0, 53.6
α, β, γ (°)	90, 90, 90	90, 90, 90	90, 94.1, 90	90, 95.2, 90
Resolution range (Å)	50–1.5 (1.53–1.50)	50–3.4 (3.46–3.40)	50–2.4 (2.44–2.40)	50–2.2 (2.24–2.20)
Total No. of reflections	287525	92097	55121	67745
No. of unique reflections	59633 (2577)	6299 (288)	13881 (700)	17067 (902)
Multiplicity	4.8 (2.4)	14.8 (15.6)	4.0 (4.1)	4.0 (4.2)
Mean $I/\sigma(I)$	40.1 (5.6)	48.8 (5.5)	25.1 (5.8)	44.1 (35.4)
Completeness (%)	98.0 (85.6)	99.5 (100.0)	97.3 (100.0)	94.9 (99.4)
R_{merge} (%)	8.4 (28.4)	10.6 (81.6)	10.1 (41.6)	5.3 (6.8)
$R_{p.i.m.}$	0.037 (0.165)	0.028 (0.205)	0.050 (0.202)	0.027 (0.033)
$CC_{1/2}$	0.996 (0.898)	0.993 (0.886)	0.992 (0.921)	0.997 (0.996)
Wilson B factor (Å^2)	13.4	119.7	28.6	19.5
Refinement				
R_{work} (%)	17.4 (19.6)	24.0 (39.6)	19.3 (21.9)	19.6 (21.5)
R_{free} (%)	21.2 (27.4)	28.3 (46.3)	26.2 (29.3)	25.8 (28.3)
R.m.s.d., bond lengths (Å)	0.006	0.011	0.011	0.008
R.m.s.d., bond angles (°)	0.967	1.403	1.356	1.235
B factor (Å^2)				
Overall	21.9	120.8	34.0	32.5
Protein	19.4	120.8	34.0	32.1
Ligand	22.5	120.9	30.7	—
Water	34.6	0	34.4	37.8
No. of non-H atoms				
Protein	3020	2957	2957	2957
Ligand	57	59	80	—
Solvent	608	0	83	193
Ramachandran statistics				
Favored (%)	98.3	94.6	98.02	97.17
Outliers (%)	0	0	0	0.28
PDB entry	7wvt	7wwg	7wwd	7wwe

ligand-bound Sfh2 were determined by molecular replacement using the predicted *AlphaFold* structure of Sfh2 as a search model. One molecule of Sfh2 was found in the asymmetric unit using *Phaser*, and the density-modified maps showed clear electron density for the bound ligands and Sfh2. The final models were refined using *Phenix* (Liebschner *et al.*, 2019; Table 1). Figures showing molecular structures were generated using *PyMOL* (https://pymol.org).

2.4. Liposome preparation and SEC analysis of Sfh2

DOPC (1,2-dioleoyl-*sn*-glycero-3-phosphocholine) and POPS (1-palmitoyl-2-oleoyl-*sn*-glycero-3-phospho-L-serine) were obtained from Avanti Polar Lipids. PI (L-α-phosphatidylinositol from soybean) and squalene were obtained from Sigma–Aldrich. For the preparation of liposomes, DOPC, POPS and PI in chloroform were mixed in the desired molar ratios, incubated at 37°C for 5 min and the solvent was evaporated under a nitrogen gas stream. The dried lipids were resuspended in 1 ml 50 m*M* HEPES pH 7.2, 120 m*M* potassium acetate (HK buffer) by vortexing. The hydrated lipid mixture was frozen and thawed five times using a water bath and cooled ethanol at −70°C. The lipid mixture was extruded ten times through a 0.1 µm polycarbonate filter. The final lipid concentration of liposomes was 2 m*M*. The lipids were added to the purified Sfh2 in a 5:1 lipid:protein molar ratio and the mixture was incubated at room temperature for 2 h. The oligomeric states of the lipid-loaded Sfh2 were then analyzed by SEC. Squalene was dissolved in DMSO. The dissolved squalene was added to the purified Sfh2 in a 5:1 squalene: protein ratio. The mixture was incubated at room temperature for 2 h and was subsequently analyzed by SEC. The monomeric form of PI (or squalene)-loaded Sfh2 was isolated from the SEC fractions and was used for protein crystallization and lipid-release assays. To examine the release of bound ligands to the acceptor liposomes and the subsequent change in the oligomeric state, Sfh2–PI (or Sfh2–squalene) was mixed with DOPC liposomes in a 50:1 lipid:protein molar ratio. After incubation at room temperature for several time intervals, samples were centrifuged at 14 000*g* for 10 min and the supernatants were analyzed by SEC.

2.5. Calculation of cavity and ligand volumes

The cavity volumes of ligand-binding sites were calculated using *Swiss-PdbViewer* with surface- and cavity-detection tools. The subpockets were identified using the option 'detect normal grooves'. The molecular volumes of PI and squalene

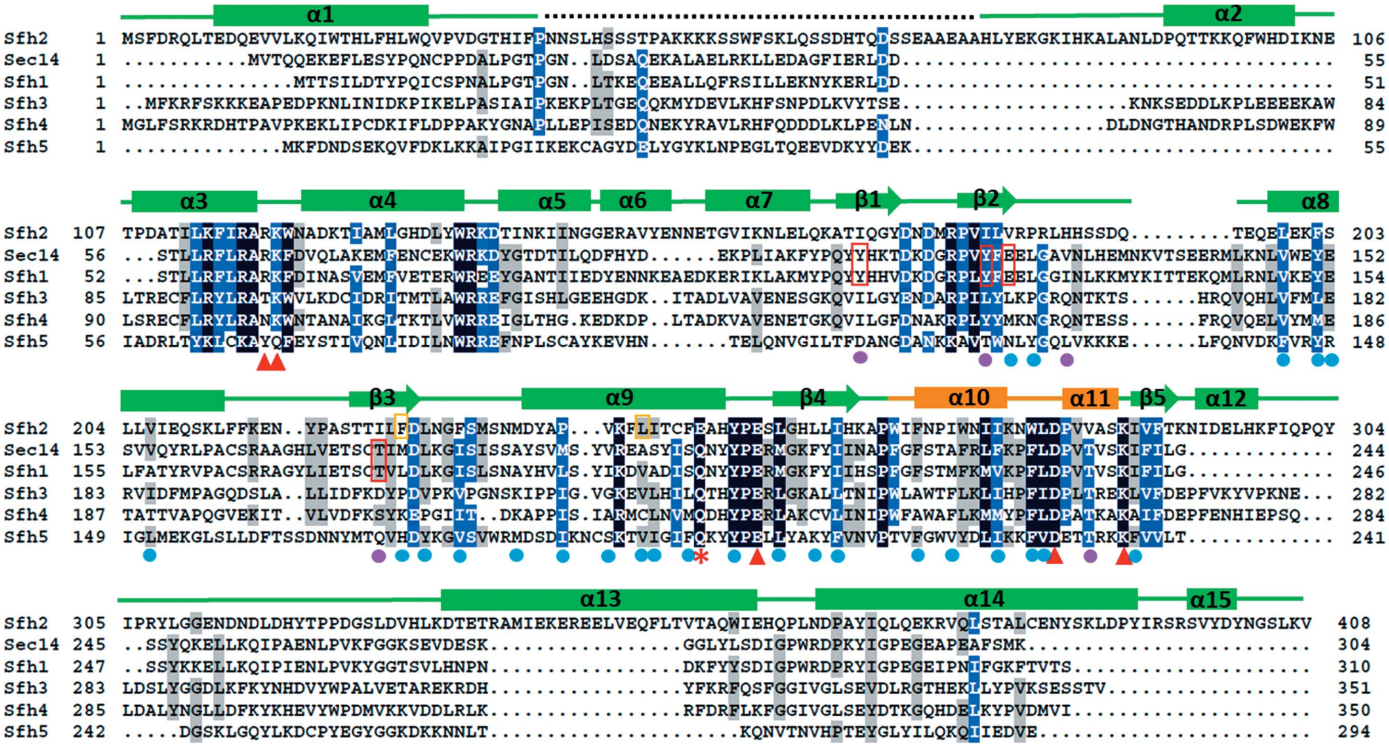

Figure 1
Sequence alignments of yeast Sec14 family proteins. Secondary-structure elements are indicated with bars and arrows for α-helices and β-strands, respectively. Orange rectangles indicate the gating helices. The dotted line indicates a disordered loop. Red triangles indicate the residues interacting with the inositol head groups of PI. The red asterisk indicates Glu249, which makes a hydrogen bond to the carbonyl group of the *sn*-1 acyl chain in Sfh2, which is unique among Sec14/Sfh proteins. Filled circles indicate the residues of the hydrophobic cavity. Purple circles indicate unique residues in the hydrophobic cavity of Sfh2. The red boxes indicate the unique residues of Sec14 and Sfh1, which interact with the polar head groups of PC and PE in the hydrophobic floor of the pocket. Orange boxes indicate the unique residues that form the toroid-shaped squalene-binding pocket.

were calculated with a probe radius of 1.4 Å using the *Volume Assessor* website (http://3vee.molmovdb.org/volumeCalc.php).

3. Results

3.1. The overall structure of Sfh2

All Sfh homologs in yeast are composed of single globular domains with large sequence variations in the N- and C-terminal regions. Sfh2, which is composed of 408 residues, is the longest homolog among yeast Sec14-like PITPs (Fig. 1). Sfh2 contains a 40-residue loop insertion between helices α1 and α2 compared with other Sfh proteins. Sfh2 has an additional C-terminal extension including α13 and α14. We purified *S. cerevisiae* Sfh2 in the apo form using an *E. coli* expression system. The flexible α1–α2 loop was susceptible to proteolytic degradation during protein purification. Therefore, we truncated 12 residues of the α1–α2 loop (residues 44–49 and 60–65), which was essential for the crystallization of Sfh2. We determined the crystal structures of Sfh2 in the apo form and in complex with its cognate ligands. Ligand-bound Sfh2 was prepared by incubating the purified Sfh2 with PI or squalene and isolating the ligand-loaded Sfh2 by SEC. Structures of Sfh2 in complex with PI and squalene were determined at 1.5 and 2.4 Å resolution, respectively, by molecular replacement using the *AlphaFold* model of apo Sfh2 (Figs. 2*a*–2*d*). The predicted *AlphaFold* model was highly similar to the experimental structures, with an r.m.s.d. of 0.53 Å for 325 equivalent C^{α} atoms (Fig. 2*e*). Electron densities for bound ligands and all backbone residues were strongly visible (Fig. 3). The truncated α1–α2 loop composed of 17 residues was disordered and was not visible in the crystal structure. The overall structure of Sfh2 contains 15 α-helices and five β-strands, which fold into two subdomains (Fig. 2*a*). The first subdomain consists of the N-terminal six α-helices (α1–α6) and the C-terminal helices α13 and α14. The second subdomain containing a large hydrophobic cavity consists of a central five-stranded β-sheet (β1–β5) surrounded by five α-helices (α7–α12). The five β-strands constitute the hydrophobic pocket floor. The α10 and α11 helices, known as the gating helices of the hydrophobic cavity, are closed in the PI- and squalene-bound structures (Figs. 2*a* and 2*b*). The cavity closed by the gating helices has a total volume of 1505 $Å^3$. The gating helices interact with helix α9 and the hydrophobic parts of PI and squalene, stabilizing the closed conformation of Sfh2.

3.2. Dimeric Sfh2 in the apo form dissociates into monomers upon substrate binding

SEC analysis of purified Sfh2 in the apo form showed two elution peaks corresponding to homodimers and monomers of Sfh2. The dimeric form constituted approximately 90% of the

purified protein (Fig. 4*a*). We collected the dimeric and monomeric fractions, incubated them at room temperature for 12 h and reanalyzed the oligomeric states of the fractions by SEC. Incubation of dimeric fractions of apo Sfh2 slowly produced a small fraction of new monomers (Fig. 4*b*). However, incubation of monomeric fractions did not produce dimers (Fig. 2*c*), suggesting that the dimer–monomer transition of apo Sfh2 is not favorable. In contrast, incubation of dimeric Sfh2 with PI or squalene shifted the oligomeric state completely into monomers (Fig. 4*a*). Squalane, the fully reduced form of squalene, also binds to Sfh2: treatment with squalane shifted dimeric apo Sfh2 into monomers in SEC (Fig. 4*a*). Incubation of dimeric Sfh2 with DOPC or DOPS liposomes did not change the oligomeric state of Sfh2, which could be explained by its lack of propensity to bind DOPC and DOPS. Similarly, recombinant Sfh3 was reported to be a dimer in a ligand-free state, and PI binding dissociates the dimer into monomers (Yang *et al.*, 2013; Yuan *et al.*, 2013). The dimer–monomer transition of Sfh3 was reversible by ligand uptake and release (Yang *et al.*, 2013). When Sfh2 monomers loaded with PI or squalene were incubated with DOPC liposomes, a significant fraction of Sfh2 co-eluted with the liposomes, but only a small fraction of dimeric Sfh2 appeared (Figs. 4*d* and 4*e*). These observations suggest that the dissociation of the Sfh2 dimer into monomers on ligand binding is efficient, while conversion back to the apo form by ligand release and subsequent dimerization was not favorable under the experimental conditions.

In addition, we determined crystal structures of monomeric Sfh2 in the apo form and dimeric PI-bound Sfh2 at 2.2 and 3.4 Å resolution, respectively (Figs. 2*c* and 2*d*). The structure of apo Sfh2 was almost identical to the closed conformation of monomeric Sfh2–PI, with a C^{α} r.m.s.d. of 0.53 Å. The configuration of the Sfh2–PI dimer was very similar to the dimeric

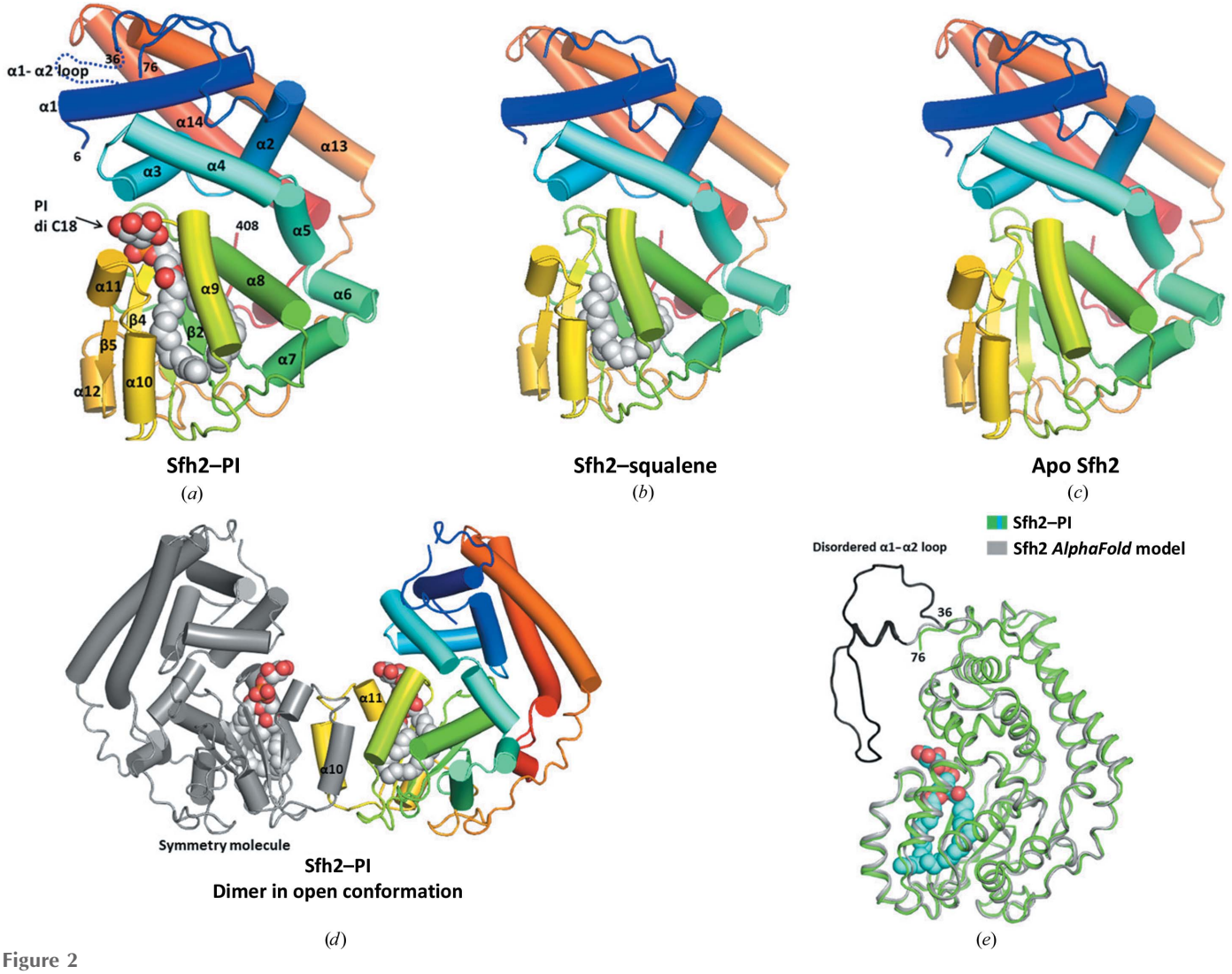

Figure 2
The overall structure of Sfh2. (*a*) The overall structure of the Sfh2–PI complex. The structure is colored blue to red from the N-terminus to the C-terminus. The disordered residues in the α1–α2 loop (residues 7–35) are indicated by dotted lines. (*b*) The structure of the Sfh2–squalene complex. (*c*) The structure of apo Sfh2. (*d*) The structure of dimeric Sfh2 in the open conformation with PI. One of the protomers shown in gray is related by a crystallographic twofold axis. (*e*) Structural comparison of the predicted *AlphaFold* model with the final Sfh2–PI model. The disordered α1–α2 loop was not included in the experimental model.

structure of Sfh3–PI reported previously (Yang *et al.*, 2013). Crystals of dimeric Sfh2–PI were obtained using the isolated monomers of Sfh2–PI. The two protomers of the dimer were related by a crystallographic twofold axis in the crystal lattice. This suggests that the dimer was formed by a dimer–monomer transition of Sfh2–PI monomers during the crystallization process. The dimer interface burying a total of 815 Å^2 of surface area is formed by the hydrophobic interaction of two gating helices in an open conformation (Fig. 4*f*). Helix α10 in the open form is located 15 Å away from its position in the closed conformation (Fig. 4*g*). The open conformation of Sfh2 exposes a hydrophobic patch on the gating helices, which could favor the association of gating helices to form a homodimer. Although the two protomers of dimeric Sfh2–PI have an open conformation of the gating helices, helix α10 from the other protomer occupies the position in which helix α10 is located in the closed form of monomeric Sfh2–PI (Fig. 4*h*). Helix α10 of the neighboring molecule makes hydrophobic interactions with helices α9 and α10, resulting in the formation of a symmetric dimer. Due to the open

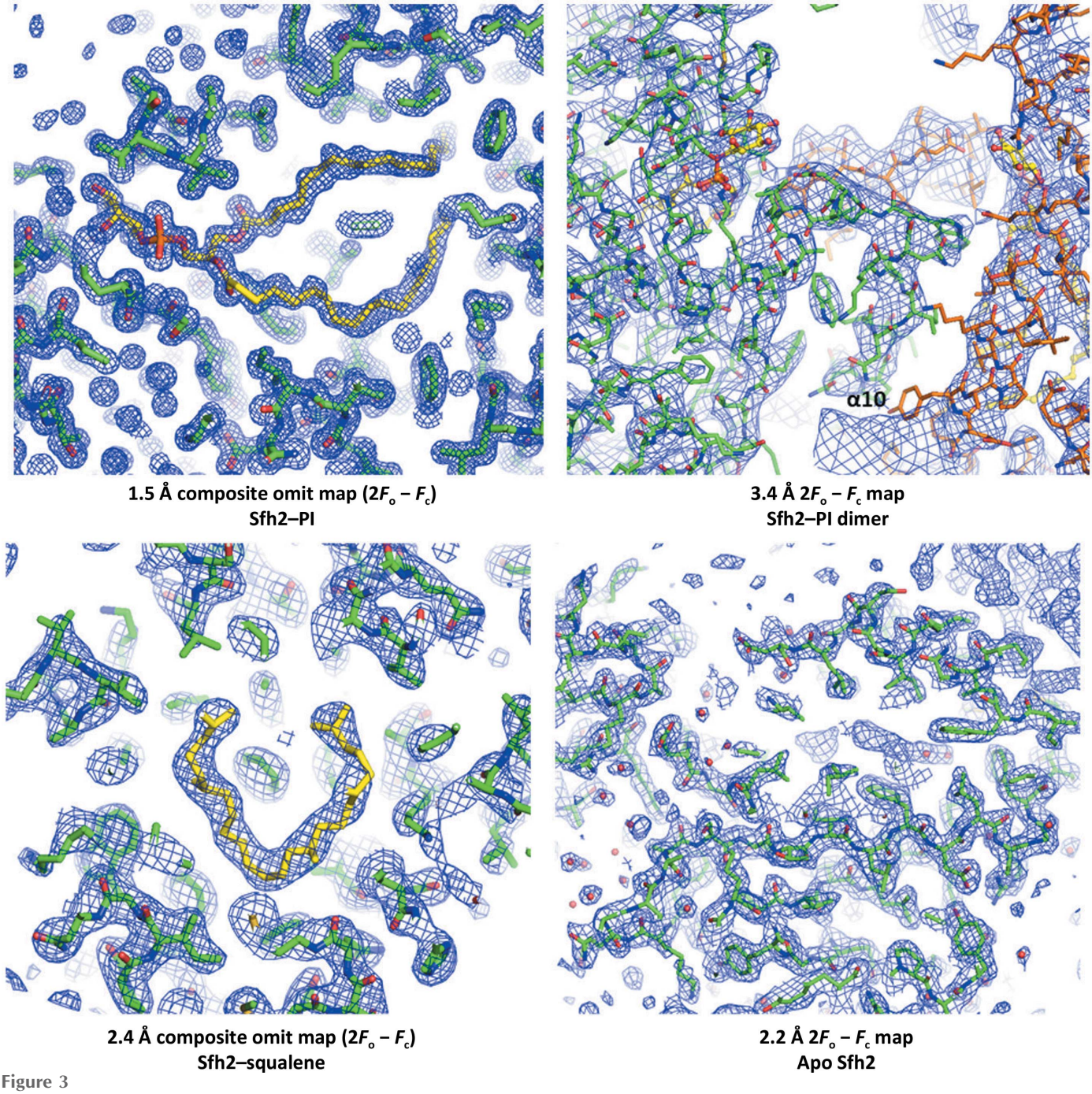

Figure 3
Electron-density maps of the crystal structures determined in this study. Composite omit maps ($2F_o - F_c$) are shown for the Sfh2–PI and Sfh2–squalene structures. The final models are shown as stick models. The proteins and ligands are colored green and yellow, respectively.

conformation, helix α10 of the symmetry molecule displays a 180° flipped orientation compared with helix α10 of the closed form. Trp278 and Ile274 of helix α10 interact with helix α9 in the closed conformation. However, in the Sfh2–PI dimer Trp278 and Ile274 of the symmetry molecule interact with the *sn*-2 acyl chain of PI. Except for the conformational variation of the gating helices, the structures of dimeric and monomeric Sfh2–PI are almost identical. Therefore, the dimeric and monomeric forms of Sfh2–PI display a very similar mode of PI binding.

The open form of Sfh2 exposes the cavity and hydrophobic patches of the gating helices. Therefore, the open form of the Sfh2 monomer is unlikely to exist in solution, but might be present during membrane association and ligand transfer. Sfh2 binds PI and squalene in a mutually exclusive manner, implying that Sfh2 could always be loaded either with PI or squalene in the cytosol except for a transient membrane-bound state. Considering the mobile nature of the hydrophobic gating helices, the physiological significance of the dimer–monomer transition of Sfh2 that is observed *in vitro* is still not clear.

3.3. Structure of the Sfh2–PI complex

The interface between the N-terminal and C-terminal subdomains creates a pocket that accommodates the inositol head group of PI. The pocket is mainly composed of hydrophilic residues from the α3–α4, α10–α11 and α9–β4 loops. The charged residues of helices α3 and α11 (Arg119, Lys120, Asp254 and Asp280) recognize the hydroxyl groups of the inositol head group. The phosphate group of PI is recognized by Lys286 and the backbone N atoms of the α9–β4 loop (Fig. 5*a*). All of the polar residues recognizing the PI head group are well conserved in Sec14-like PITPs, indicating that

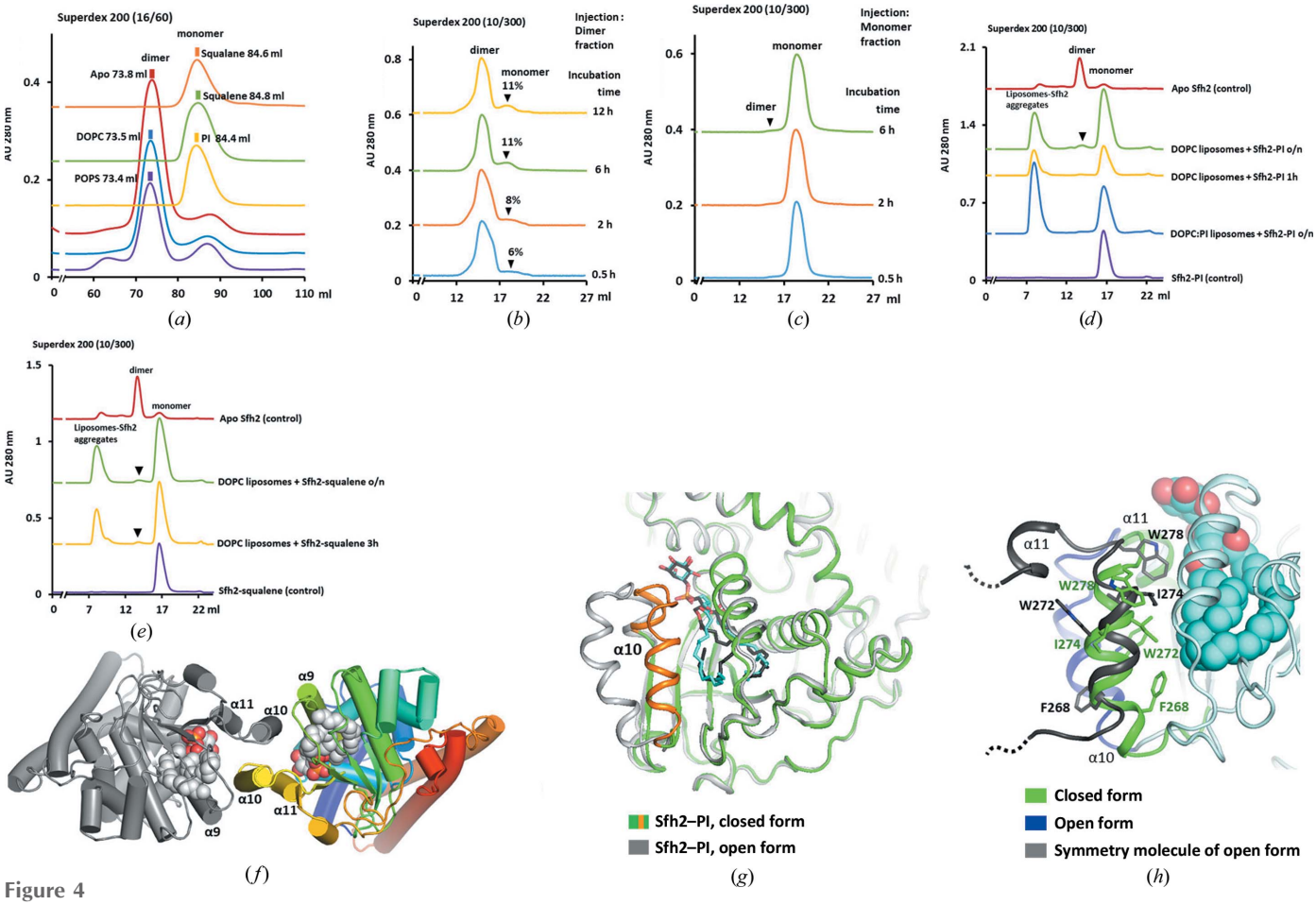

Figure 4

The dimer–monomer transition of purified Sfh2. (*a*) SEC profiles of the purified Sfh2 proteins incubated with various lipids. (*b*) The dimeric fractions collected from the first SEC were incubated at room temperature for several time intervals prior to SEC analysis to examine the dimer–monomer equilibrium. The appearance of a monomeric peak is indicated by black triangles and the percentages of monomeric species are shown. (*c*) The fractions collected from the monomeric peak of apo Sfh2 were reanalyzed by SEC to examine the dimerization. (*d*) SEC profiles of Sfh2–PI incubated with DOPC liposomes. 1 mg of PI-loaded Sfh2 was mixed with 2 m*M* of the stock liposomes in a 1:50 molar ratio, resulting in a 0.01 m*M* final protein concentration, and incubated for 14 h prior to SEC analysis. DOPC:PI liposomes contain a 9:1 molar ratio of DOPC and PI. The black filled triangle indicates the elution peak of dimeric Sfh2. (*e*) SEC profiles of Sfh2–squalene incubated with DOPC liposomes. (*f*) The structure of the crystallographic dimer of Sfh2–PI. Helix α10 in an open conformation from each protomer covers the hydrophobic pocket of the other protomer, forming a dimer interface in the center. (*g*) Structural comparison of the closed and open forms of the Sfh2–PI complex. (*h*) Comparison of the conformations of the gating helices in the closed and open forms. The gating helices from the open form, closed form and a symmetry molecule of the open form are shown in blue, green and gray, respectively.

PI is the common ligand in this protein family (Fig. 1). Two acyl chains of PI, each consisting of 18 C atoms, fill the entire length of the hydrophobic cavity by extending to the bottom (Fig. 5*b*). PI, with a molecular volume of 1208 Å^3, occupies 80% of the cavity volume. The acyl chains of PI are well ordered in the pocket by extensive hydrophobic interactions with the cavity walls. The bound PI is almost completely buried in the binding cavity (Fig. 5*c*). The 4-hydroxyl group of the inositol ring is only partially exposed to the solvent. Therefore, phosphoinositides cannot bind to the pocket due to steric clashes between the phosphate groups and the binding pocket. Unlike other Sec14 family proteins, the deep cavity of Sfh2 is composed of hydrophobic residues, which permit the binding of only hydrophobic groups.

Structural comparison of Sfh2 with Sfh3 and other Sec14 homologs suggests that the binding mode of PI is highly conserved (Fig. 5*d*). While the N-terminal subdomain is relatively variable, the backbones of the ligand-binding domains are highly conserved in Sfh homologs (Fig. 6). Most of the residues that interact with the hydrophilic head groups of PI are well conserved in Sec14/Sfh proteins. The conformations of the PI head groups in Sfh2 and Sfh3 are almost identical,

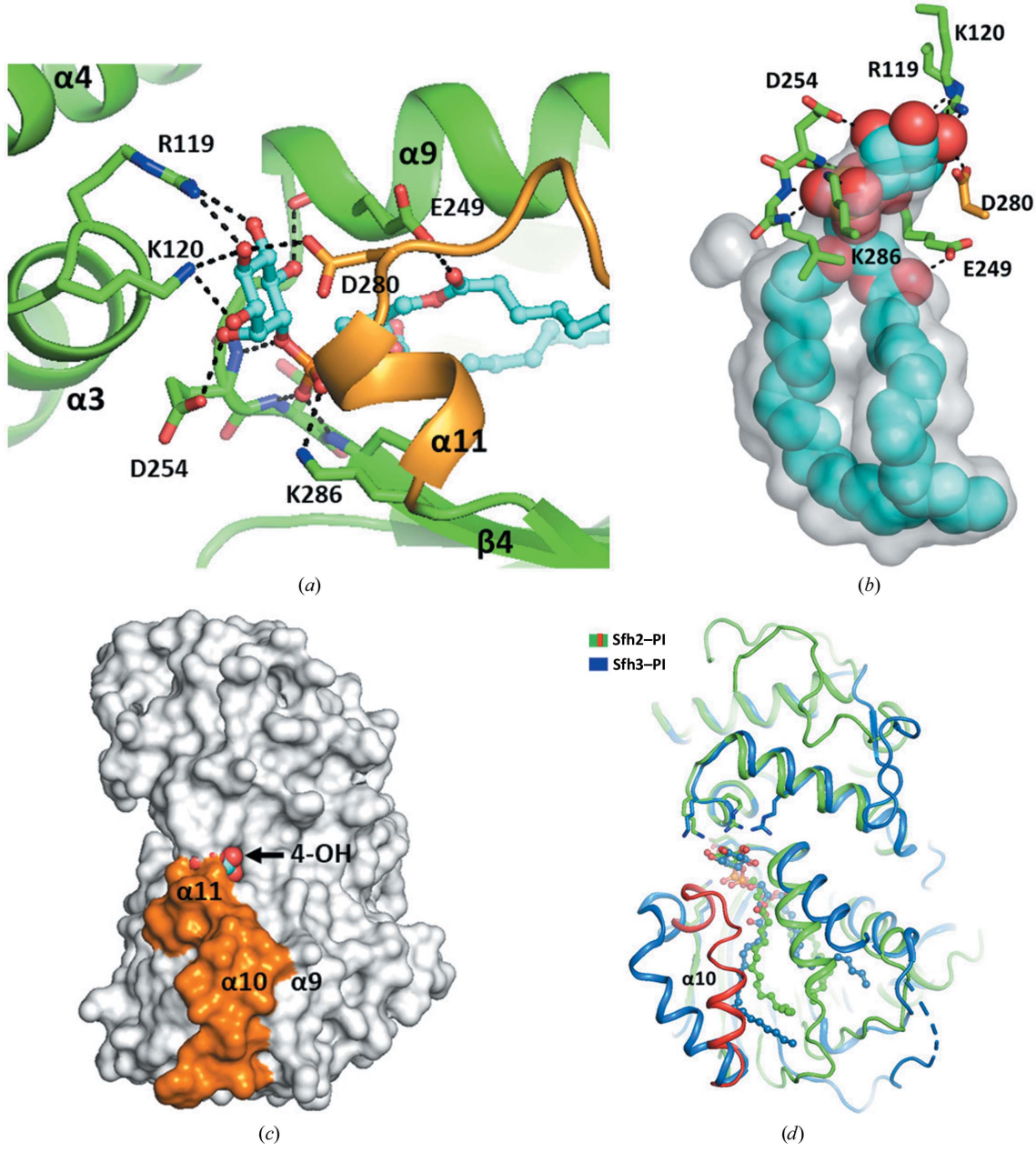

Figure 5
PI-binding site of Sfh2. (*a*) The hydrogen-bonding network between the inositol head group and Sfh2 residues is shown by dashed lines. The gating helices are colored orange. (*b*) A surface representation of the PI-binding cavity. The residues recognizing the inositol head group are shown as stick models. (*c*) Surface representation of Sfh2–PI. The gating helices, α10 and α11, are colored orange. The bound PI is shown as a sphere model. The 4-hydroxyl group of the inositol head group is indicated by an arrow. (*d*) Structural comparison of PI-bound Sfh2 and Sfh3. The gating helices of Sfh2 are indicated in red. One protomer of the Sfh3–PI dimer is shown with an open conformation of the gating helices.

indicating strict conservation of ligand recognition (Fig. 5*d*). The side chain of Glu249 makes a hydrogen bond to the carbonyl group of the *sn*-1 acyl chain in Sfh2 (Fig. 5*a*). However, all other Sec14/Sfh proteins have a Gln residue in the equivalent positions, explaining the conformational variation of the glycerol backbones of PI compared with other Sfh proteins. The orientations of the two acyl chains of PI in Sfh2 are extended in parallel, while the two acyl chains in Sfh3 are separated in the wide hydrophobic cavity (Fig. 5*d*). The variation in the hydrophobic cavity suggests that Sfh homologs might accommodate many PI species with acyl chains of different lengths.

3.4. Recognition of squalene

Sfh2 displays a toroid-shaped hydrophobic cavity, which is shape-complementary to the folded squalene (Fig. 7*a*). Squalene binds in the pocket with a V-shaped conformation. Squalene occupies the bottom of the cavity, occupying 49% of the total cavity volume. 28 hydrophobic residues in the deep cavity of Sfh2 compose the toroid-shaped pocket (Fig. 7*b*). In particular, Phe226, Leu244 and Phe248 are unique residues in Sfh2 that form the shape of the hydrophobic cavity (Fig. 1). Binding of squalene to the shape-complementary pocket is mediated entirely by hydrophobic interactions (Fig. 7*b*). Despite the lack of specific hydrogen-bonding contacts between squalene and Sfh2, squalene is well ordered in the binding pocket, with clear electron density (Fig. 3). The hydrophobic residues of α8, α9, α10 and the floor of the cavity (β1–β5) contribute to squalene binding. All water molecules are excluded from the deep cavity in ligand-bound forms. The binding of squalene overlaps with the binding sites of the *sn*-1 acyl chain and half of the *sn*-2 acyl chain of PI (Fig. 7*c*). Compared with PI-bound Sfh2, Sfh2–squalene displays

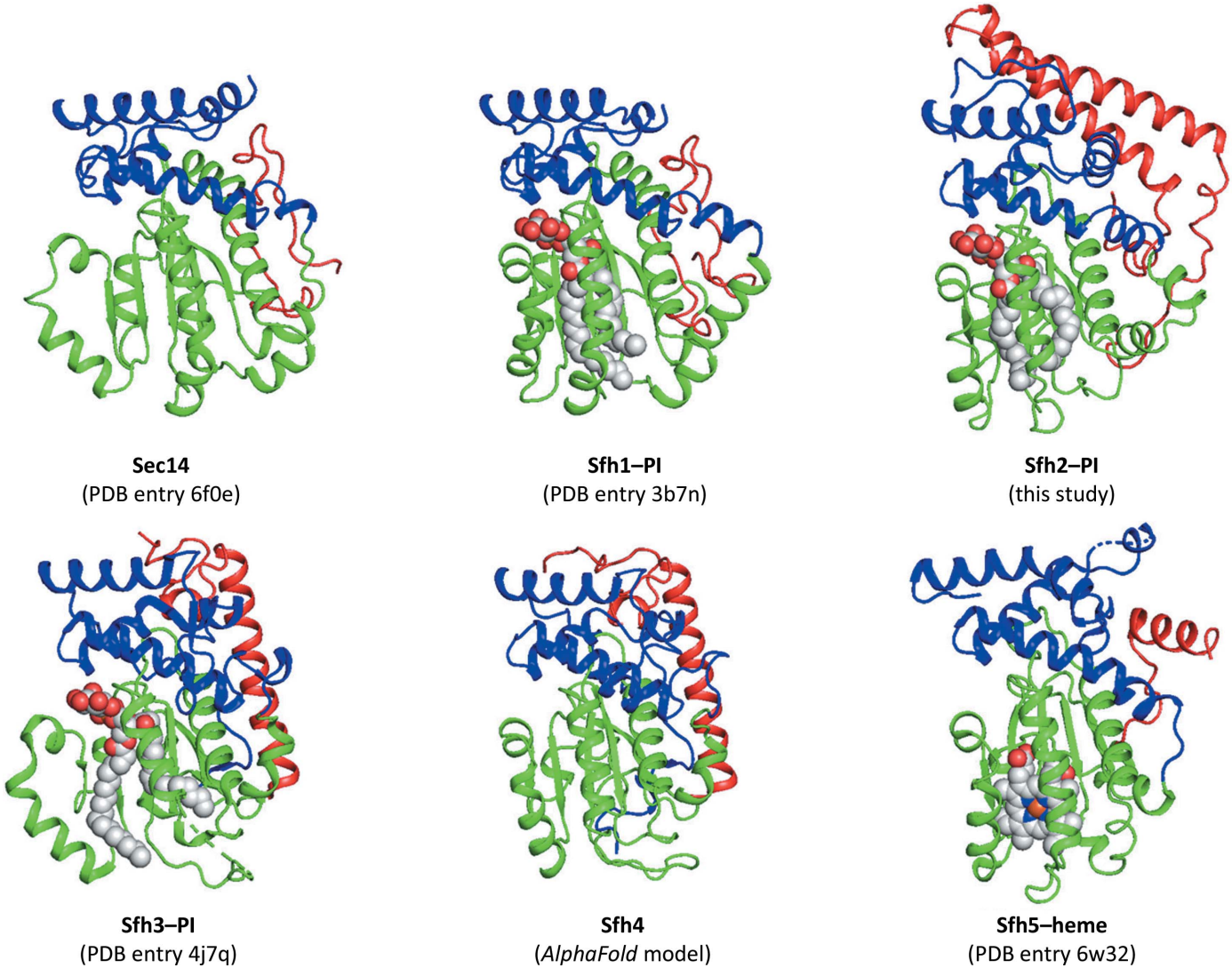

Figure 6
Structures of Sec14-like PITPs. The experimental structures of Sec14-like PIPTs are shown as ribbon models. An *AlphaFold* model is shown for the Sfh4 homolog. The N-terminal helical subdomains are colored blue. The middle ligand-binding domain is shown in green and the C-terminal extension is shown in red.

conformational differences in the side chains of Arg119 and Lys120 which recognize the inositol head group (Fig. 7*d*). The squalene-bound form has a 310 Å^3 smaller cavity volume than PI-bound Sfh2 to accommodate the small squalene molecule (Figs. 7*c* and 7*d*). The contacts with the hydrophobic acyl chains of PI and squalene result in a small conformational difference of the side chains of Met236, Leu256 and Leu259 in the cavity wall (Fig. 7*c*). In addition, the side chain of Phe248 moves towards the cavity in the squalene-bound form. The structural differences between Sfh2–PI and Sfh2–squalene are limited, with a C$^{\alpha}$ r.m.s.d. of 0.47 Å, suggesting that the binding pocket is predetermined to bind either PI or squalene without significant conformational changes of the backbone atoms (Fig. 7*d*). In conclusion, the specific hydrophobic residues in the ligand-binding cavity dictate the binding of squalene by Sfh2.

3.5. Squalene specificity of Sfh2

To investigate the structural determinants of squalene specificity, we compared the ligand-binding modes of human supernatant protein factor (SPF) and Sfh2. SPF belongs to the CRAL-TRIO family of lipid-binding proteins, which includes yeast Sec14-like PITPs and human tocopherol transfer proteins. SPF contains an N-terminal Sec14-like domain displaying squalene-binding activity and a C-terminal eight-stranded barrel (Stocker *et al.*, 2002; Christen *et al.*, 2015). The lipid-binding domains show 24% sequence identity for 150

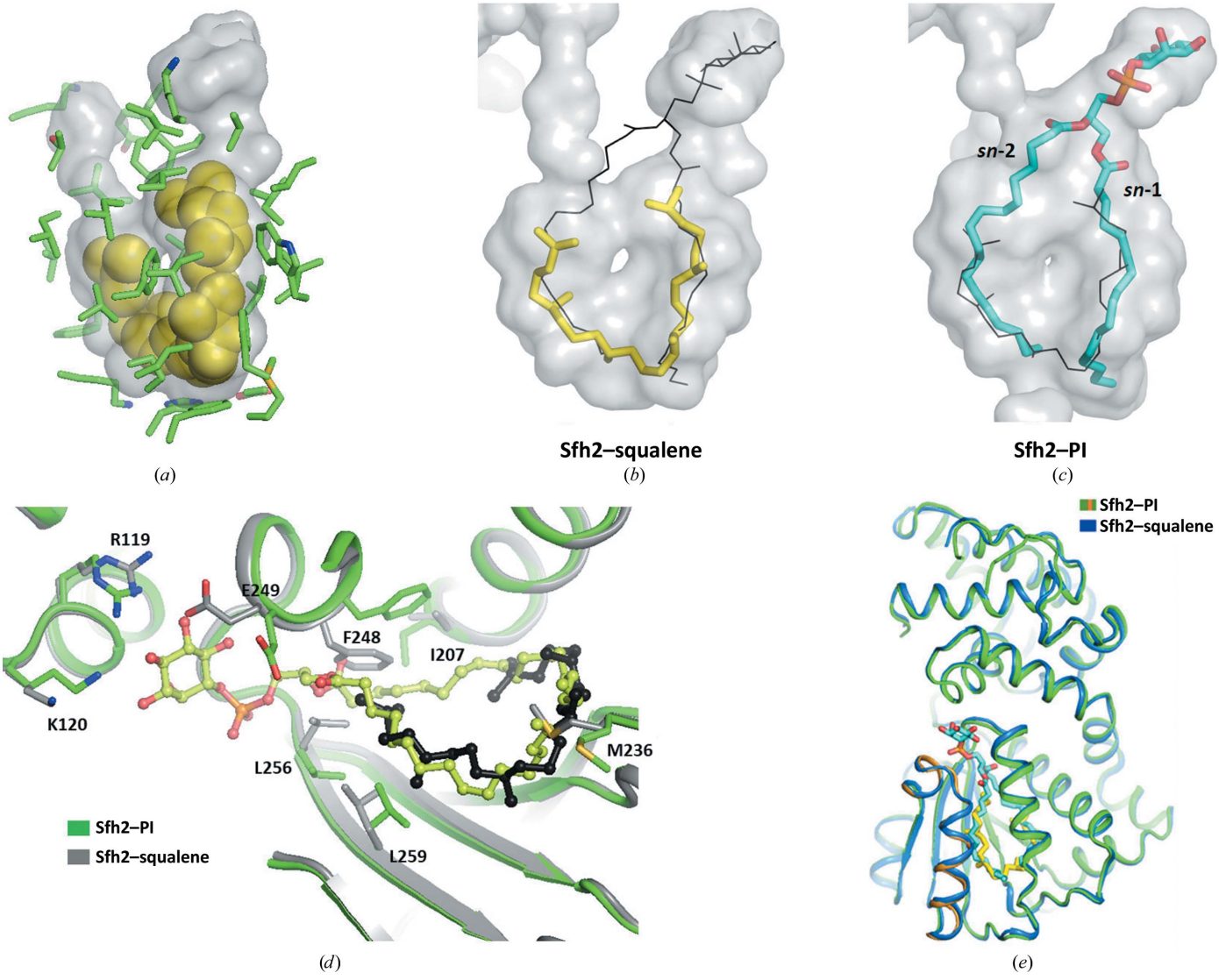

Figure 7
Squalene-binding site of Sfh2. (*a*) Squalene in the hydrophobic cavity. The residues composing the hydrophobic cavity are shown as stick models. The cavity is shown as a transparent surface. Superposition of bound PI and squalene in the cavity. (*b*) The hydrophobic cavity of squalene-bound Sfh2. The bound squalene is colored yellow and the position of PI is indicated by black lines. (*c*) The ligand-binding cavity of Sfh2–PI is shown as a transparent surface and the bound PI is shown as a stick model. Squalene is shown as black lines to show the overlapping binding sites. (*d*) Structural comparison of the ligand-binding sites of Sfh2–PI and Sfh2–squalene. The residues showing the conformational differences between the PI and squalene structures are shown as stick models. (*e*) Structural comparison of PI- and squalene-bound Sfh2. PI is colored in cyan and squalene is shown as a yellow stick model.

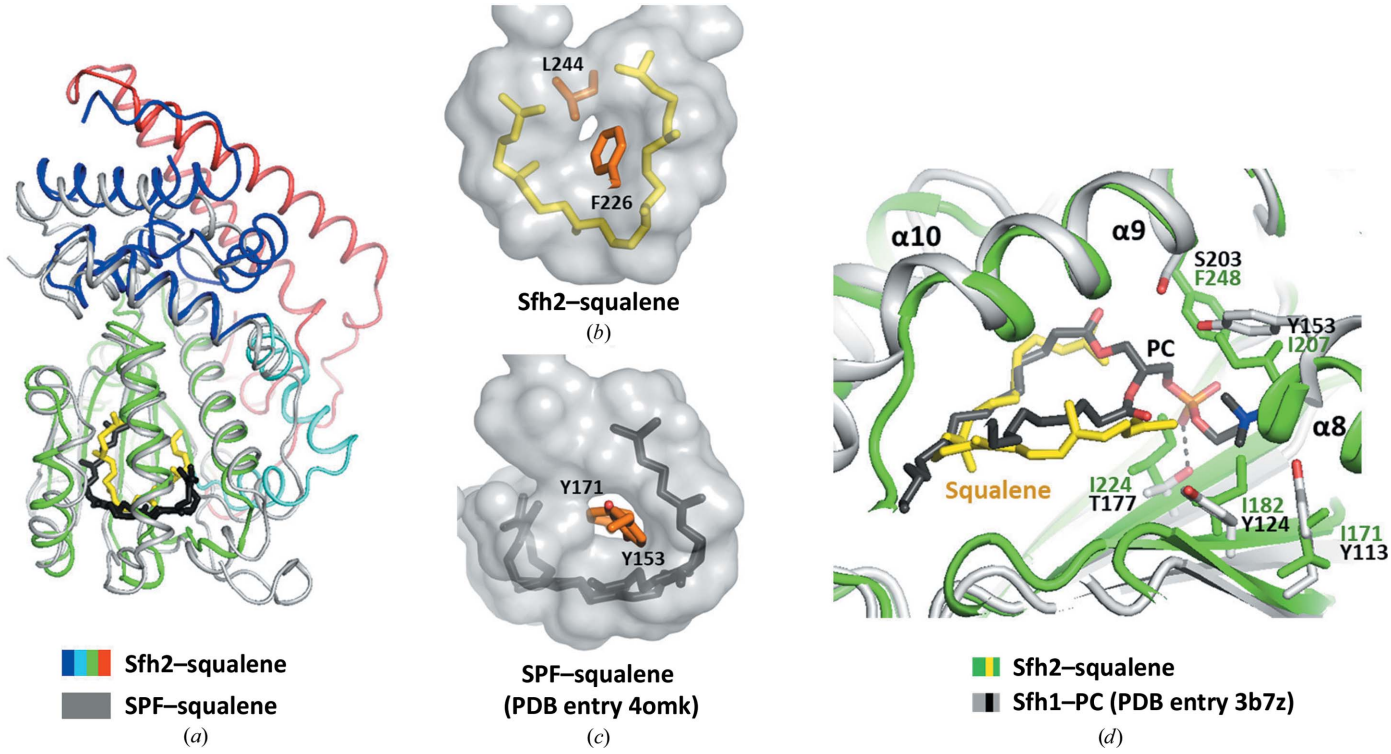

Figure 8
(*a*) Structural comparison of Sfh2–squalene and SPF–squalene. (*b*) The hydrophobic cavity of Sfh2 is shown as a transparent surface. Squalene is shown as yellow sticks. The two bulky residues in the center of the cavity are shown as stick models. (*c*) The hydrophobic cavity of SPF is shown as a transparent surface. Squalene is shown as gray sticks. (*d*) Structural comparison of the ligand-binding sites of Sfh2–squalene and Sfh1–PC (PDB entry 3b7z). The key residues of Sfh1 interacting with the PC head group are shown as stick models. The equivalent residues of Sfh2 are shown.

equivalent residues. The structures of the lipid-binding domains of Sfh2 and SPF are well conserved, with a C^{α} r.m.s.d. of 3.6 Å, while the N-terminal subdomains and C-terminal extension are highly variable (Fig. 8*a*). Both Sfh2 and SPF have toroid-shaped hydrophobic cavities, with similar volumes of 1195 and 1176 $Å^3$, respectively (Figs. 8*b* and 8*c*). The toroid shape arises from the presence of two bulky hydrophobic residues in the center of the cavity. Phe226 in the floor of the cavity and Leu244 in the ceiling of the cavity in Sfh2 narrow the center of the cavity, forming a toroid-shaped binding pocket (Fig. 8*b*). In SFP, Tyr153 and Tyr171 in the center of the cavity play an equivalent role in shaping the hydrophobic cavity (Fig. 8*c*). The bound squalene molecule displays a V-shaped conformation in Sfh2 (Fig. 8*b*) and shows a U-shaped conformation in SFP (Figs. 8*b* and 8*c*). Squalene in Sfh2 is well ordered in the binding pocket with one conformation, while squalene bound to SPF shows flexibility with dual conformations (Christen *et al.*, 2015).

Yeast Sfh3 is known to bind and transport ergosterol as a secondary ligand (Tripathi *et al.*, 2019; Holič *et al.*, 2014). In Sfh2, the small dimensions and the unique shape of the hydrophobic cavity exclude the binding of ergosterol-containing rigid hydrocarbon rings. In the β-sheet floor of the cavity, Sfh2 lacks the hydrophilic residues which can recognize the polar head groups of PC and phosphatidylethanolamine (PE) in Sec14, Sfh1 and Sfh3 (Fig. 1). For example, Tyr113 and Thr177, which make hydrogen bonds to the head group of PE in Sfh1, are replaced by Ile171 and Ile224, respectively, in Sfh2 (Fig. 7*c*). Tyr124 and Tyr153 of Sfh1 stabilize the choline head group of PC by cation–π interactions. These aromatic residues are replaced by Ile182 and Ile207 in Sfh2, correlating with the lack of PC binding in Sfh2. In conclusion, both Sfh2 and SPF display shape-complementary binding cavities composed of almost entirely hydrophobic residues, explaining their specificity for squalene and the lack of PE, PC and sterol binding.

4. Discussion

Ergosterol is one of the major lipid components of the yeast plasma membrane, accounting for 50% of the lipid content (van Meer *et al.*, 2008). Ergosterol biosynthesis is controlled by tight regulation of the key rate-limiting enzymes HMG-CoA reductase and squalene monooxygenase (also known as squalene epoxidase; Yoshioka *et al.*, 2020; Foresti *et al.*, 2013). Squalene is known to upregulate squalene monooxygenase activity via allosteric modulation of its stability (Yoshioka *et al.*, 2020). A link between Sfh2 and sterol metabolism in yeast has been reported, showing that expression of the SUT1 (sterol uptake protein 1) transcription factor involved in sterol utilization suppresses *sec14-1* through the upregulation of Sfh2 (Régnacq *et al.*, 2002). In addition, Sfh2-knockout yeast cells exhibit an enhanced sensitivity to terbinafine, an inhibitor of squalene monooxygenase (Tripathi *et al.*, 2019). Squalene is found in the lipid droplets (LDs) and between membrane leaflets due to its highly hydrophobic nature (Spanova *et al.*, 2010). Accumulation of squalene in yeast leads to clustering of

lipid droplets and thereby may affect the growth and distribution of lipid droplets (Ta *et al.*, 2012).

Sfh2 displays structural similarity to human supernatant protein factor (SPF), which facilitates the access of squalene to the monooxygenase in cholesterol biosynthesis (Christen *et al.*, 2015). Sfh2 shows a conserved mode of squalene binding with the Sec14-like domain of SPF. Considering the lipid-transport role of Sfh2 *in vitro* (Tripathi *et al.*, 2019), the distribution of squalene within the subcellular organelles might be mediated by Sfh2 facilitating substrate flow to and from squalene monooxygenase. Alternatively, Sfh2 might sense the squalene level and translate the metabolic information into phosphoinositide signaling. However, no direct proof has been reported for a squalene-transport role of Sfh2 *in vivo*. How squalene and PI transport are coupled to its biological function remains elusive.

Heterotypic lipid exchange was proposed as the common role of Sec14-like PITPs, counter-transporting PI as a common substrate and secondary lipids such as PC and squalene (Tripathi *et al.*, 2019). Sec14-like PITPs have been reported to exist in two conformations generated by hinge movement of the gating helices. The open form represents the conformation involved in lipid exchange on membrane surfaces since it exposes the hydrophobic pocket suitable for membrane binding and lipid extraction. Recombinant Sfh2 in a ligand-free state formed a dimer. The apo form favors an open conformation due to a lack of interaction between the ligand and gating helices, which seems to induce association of Sfh2 monomers by hydrophobic interaction of the gating helices. However, the ligand-binding pocket of Sfh2 *in vivo* seems to always be occupied by either PI or squalene during the ligand-transfer cycles, except for the transient membrane-bound state for lipid exchange. For Sfh2, the transport of PI from the donor membrane to the acceptor membrane might require the delivery of squalene back to the donor membrane to complete a heterotypic lipid-transfer cycle.

The structures of Sfh2 in this study provide accurate details of PI and squalene recognition in the ligand-binding pocket. Despite the overall fold of the ligand-binding domains being well conserved in Sec14 family proteins, the variation of the hydrophobic cavity determines the specificity for a secondary ligand and its unique biological function. The results described here are consistent with the heterotypic lipid-transfer model of Sfh2. How the distinct dual ligand specificity and the heterotypic transport of Sfh2 translate into its biological function requires further investigation.

Funding information

This work was supported by a National Research Foundation of Korea (NRF) grant funded by the Ministry of Education, Science and Technology (Grant No. 2019R1A2C1085530) and a grant from the Ministry of Oceans and Fisheries R&D project, Korea (Grant No. 2021633).

References

Balla, T. (2013). *Physiol. Rev.* **93**, 1019–1137.
Christen, M., Marcaida, M. J., Lamprakis, C., Aeschimann, W., Vaithilingam, J., Schneider, P., Hilbert, M., Schneider, G., Cascella, M. & Stocker, A. (2015). *J. Struct. Biol.* **190**, 261–270.
Desfougères, T., Ferreira, T., Bergès, T. & Régnacq, M. (2008). *Biochem. J.* **409**, 299–309.
Dickson, E. J. & Hille, B. (2019). *Biochem. J.* **476**, 1–23.
Foresti, O., Ruggiano, A., Hannibal-Bach, H. K., Ejsing, C. S. & Carvalho, P. (2013). *eLife*, **2**, e00953.
Grabon, A., Bankaitis, V. A. & McDermott, M. I. (2019). *J. Lipid Res.* **60**, 242–268.
Holič, R., Šimová, Z., Ashlin, T., Pevala, V., Poloncová, K., Tahotná, D., Kutejová, E., Cockcroft, S. & Griač, P. (2014). *Biochim. Biophys. Acta*, **1841**, 1483–1490.
Khan, D., Lee, D., Gulten, G., Aggarwal, A., Wofford, J., Krieger, I., Tripathi, A., Patrick, J. W., Eckert, D. M., Laganowsky, A., Sacchettini, J., Lindahl, P. & Bankaitis, V. A. (2020). *eLife*, **9**, e57081.
Khan, D., Nile, A. H., Tripathi, A. & Bankaitis, V. A. (2021). *Int. J. Mol. Sci.* **22**, 6754.
Li, X., Routt, S. M., Xie, Z., Cui, X., Fang, M., Kearns, M. A., Bard, M., Kirsch, D. R. & Bankaitis, V. A. (2000). *Mol. Biol. Cell*, **11**, 1989–2005.
Liebschner, D., Afonine, P. V., Baker, M. L., Bunkóczi, G., Chen, V. B., Croll, T. I., Hintze, B., Hung, L.-W., Jain, S., McCoy, A. J., Moriarty, N. W., Oeffner, R. D., Poon, B. K., Prisant, M. G., Read, R. J., Richardson, J. S., Richardson, D. C., Sammito, M. D., Sobolev, O. V., Stockwell, D. H., Terwilliger, T. C., Urzhumtsev, A. G., Videau, L. L., Williams, C. J. & Adams, P. D. (2019). *Acta Cryst.* D**75**, 861–877.
Meer, G. van, Voelker, D. R. & Feigenson, G. W. (2008). *Nat. Rev. Mol. Cell Biol.* **9**, 112–124.
Pemberton, J. G., Kim, Y. J., Humpolickova, J., Eisenreichova, A., Sengupta, N., Toth, D. J., Boura, E. & Balla, T. (2020). *J. Cell Biol.* **219**, e201906130.
Régnacq, M., Ferreira, T., Puard, J. & Bergès, T. (2002). *FEMS Microbiol. Lett.* **216**, 165–170.
Schaaf, G., Ortlund, E. A., Tyeryar, K. R., Mousley, C. J., Ile, K. E., Garrett, T. A., Ren, J., Woolls, M. J., Raetz, C. R., Redinbo, M. R. & Bankaitis, V. A. (2008). *Mol. Cell*, **29**, 191–206.
Schnabl, M., Oskolkova, O. V., Holic, R., Brezná, B., Pichler, H., Zágorsek, M., Kohlwein, S. D., Paltauf, F., Daum, G. & Griac, P. (2003). *Eur. J. Biochem.* **270**, 3133–3145.
Spanova, M., Czabany, T., Zellnig, G., Leitner, E., Hapala, I. & Daum, G. (2010). *J. Biol. Chem.* **285**, 6127–6133.
Stocker, A., Tomizaki, T., Schulze-Briese, C. & Baumann, U. (2002). *Structure*, **10**, 1533–1540.
Strahl, T. & Thorner, J. (2007). *Biochim. Biophys. Acta*, **1771**, 353–404.
Ta, M. T., Kapterian, T. S., Fei, W., Du, X., Brown, A. J., Dawes, I. W. & Yang, H. (2012). *FEBS J.* **279**, 4231–4244.
Tripathi, A., Martinez, E., Obaidullah, A. J., Lete, M. G., Lönnfors, M., Khan, D., Soni, K. G., Mousley, C. J., Kellogg, G. E. & Bankaitis, V. A. (2019). *J. Biol. Chem.* **294**, 19081–19098.
Wang, Y., Yuan, P., Grabon, A., Tripathi, A., Lee, D., Rodriguez, M., Lönnfors, M., Eisenberg-Bord, M., Wang, Z., Man Lam, S., Schuldiner, M. & Bankaitis, V. A. (2020). *J. Cell Biol.* **219**, e201907128.
Wong, L. H., Gatta, A. T. & Levine, T. P. (2019). *Nat. Rev. Mol. Cell Biol.* **20**, 85–101.
Wong, T. A., Fairn, G. D., Poon, P. P., Shmulevitz, M., McMaster, C. R., Singer, R. A. & Johnston, G. C. (2005). *Proc. Natl Acad. Sci. USA*, **102**, 12777–12782.
Yang, H., Tong, J., Leonard, T. A. & Im, Y. J. (2013). *FEBS Lett.* **587**, 1610–1616.
Yoshioka, H., Coates, H. W., Chua, N. K., Hashimoto, Y., Brown, A. J. & Ohgane, K. (2020). *Proc. Natl Acad. Sci. USA*, **117**, 7150–7158.
Yuan, Y., Zhao, W., Wang, X., Gao, Y., Niu, L. & Teng, M. (2013). *Acta Cryst.* D**69**, 313–323.